

A 3D Simulation of Glancing Angle Deposition

Ojas Kulkarni

Department of Electrical and
Computer Engineering
University of Utah

Salt Lake City, United States of
America

ojas.ajay.kulkarni@gmail.com

Chuang Qu

Department of Electrical and
Computer Engineering
University of Louisville

Louisville, United States of
America

chuang.qu@louisville.edu

Kevin Walsh

Department of Electrical and
Computer Engineering
University of Louisville

Louisville, United States of
America

kevin.walsh@louisville.edu

Shamus McNamara

Department of Electrical and
Computer Engineering
University of Louisville

Louisville, United States of
America

shamus.mcnamara@louisville.edu

Abstract—In this work, we develop a 3-dimensional simulation for a nanostructure growth technique called glancing angle deposition (GLAD). GLAD is a physical vapor deposition process capable of creating nanostructures. GLAD can be used to create sub-100 nm nanofeatures like chevrons, ribbons, columns, helices, and combinations. These structures are formed by ballistic shadowing of particle islands where the vapor flux is unable to land in this shadowed region. However, the visualization of the feature formation mechanism during GLAD is lacking. For the simulation, we utilize Python and incorporate its visual graphics module - VPython - to simulate the growth of these nanostructures in a 3D environment to visualize the GLAD process. We first simulate the deposition of natural seeds on the substrate. Then as shadows are cast from these seeds, the subsequent layers of particles being deposited onto the substrate are simulated. The simulated results of percent coverage and seed size with respect to different inputs such as varying incidence angles, rotation rate, and deposition rates are demonstrated. Additional support for different seeding schemes including cube seeds, line seeds, and sphere seeds are also presented. Our collision resolution algorithm has a time complexity of $O(sn^3)$ where s is the total number of simple features (columns) to make a complex feature. The simulation results are qualitatively agreed with our experimental results; a quantitative comparison between our simulated incidence angle and theoretical ones shows good accordance. Overall, this work demonstrates the simulated growth of GLAD thin films in a Monte-Carlo fashion to predict the fabrication result, which can be used to further guide the design of 3D GLAD nanofeature arrays for application fields such as sensing, optics, and mechanics.

Keywords—Glancing Angle Deposition, Simulation, Monte-Carlo, Thin Films, Nanostructures, Physical Vapor Deposition

I. INTRODUCTION

Glancing angle deposition (GLAD) is a bottom-up physical vapor deposition technique used to create nanostructures. GLAD has extensively studied applications in optics, sensing, magnetic storage technologies, and various other fields [1]. These nanostructures are of a sub-1 μm range.

A. Theory of GLAD

During the GLAD process, the substrate azimuth rotation angle (φ) and the incidence angle of the vapor can be manipulated in discrete or continuous time steps. These differing time steps can create structures like chevrons, helices, etc. As the incoming vapor is deposited on the substrate, the constituent particles join due to molecular/atomic interactions. This cluster of particles create sites of nucleation, called seeds which eventually form particle islands. These islands create a shadowing effect which prevents the further growth of particle islands inside this shadowed region.

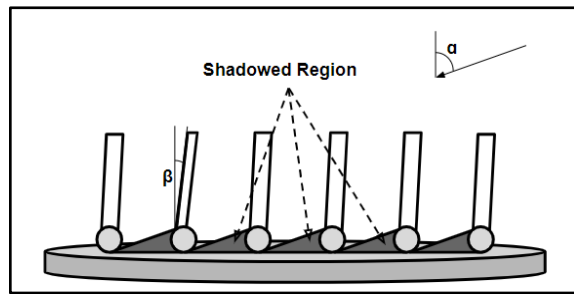


Fig. 1.1: Nanostructures on substrate with their corresponding incidence angle and the growth angle

Fig. 1.1 shows these different aspects of the GLAD process. The incident angle, α , and the column growth angle, β , are found to be significantly different. It is also accepted that $\beta < \alpha$ in all cases [2]. There have been various attempts to describe the relationship between β and α , but no universal solution exists. As expressed in [2], this derived solution gives a first-order approximation for the relationship between the two.

$$\beta = \alpha - \sin^{-1}\left(\frac{1-\cos(\alpha)}{2}\right) \quad (1)$$

In the rest of this work (1) will be used for the theoretical β calculations.

B. Exploration of Different Simulation Approaches

The approach presented in this paper is a Monte-Carlo (MC) style simulation, but molecular dynamic (MD) simulations have also been proposed. As seen in [3], this MD simulation uses hardware acceleration to achieve their goal of simulating. Also, as seen in [3], the simulation took greater than 100 hours to completely render even when using a GPU for acceleration. Our goal was to create a simulation that can be used on a CPU in a feasible amount of time. However, the rendering time has an accuracy tradeoff.

C. Research Goal

As shown in the previous section, other research groups have investigated the use of MD and MC simulations each with their own advantages. On the other hand, a 3D MC visualization has not been thoroughly studied. Thus, our goal for this research project was to implement a 3-dimensional simulation of the glancing angle deposition process in a Monte-Carlo fashion. In addition to this, one of our goals was also to keep the implementation as simple as possible so that it can be easily replicated. Another goal was to characterize the accuracy of the simulation as compared to experimental results.

II. SIMULATION

A. Modulation of the Incidence Angle

The first step to implementing such a simulation is to be able to change the incidence angle of the incoming vapor flux. An α was provided as an input to the user. To use this, two approaches were taken: a point source, and columnar vapor. As different α were chosen, the point source changed its position over the substrate as shown in Fig. 2.1.

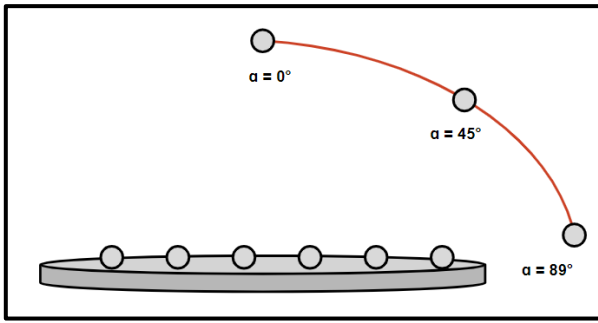


Fig. 2.1: Path of the point source as incidence angle is modulated

This point source was used as the crucible position relative to the substrate. Each particle had a different velocity vector. The other approach – the columnar vapor was achieved in a similar way. A bounding area was continuously defined for each angle. As shown in Fig. 2.2, the orientation of this bounding area was changed depending on the incidence angle.

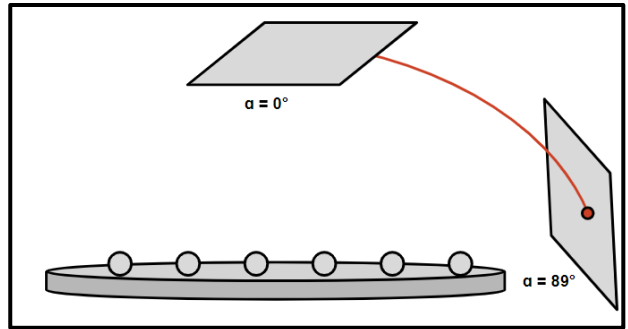


Fig. 2.2: Orientation of the bounding area for columnar vapor flux

In this approach for setting the incidence angle, the velocity of all particles in the bounding area is the same. It is ensured that all the particles will land on the substrate instead of missing it.

B. Collision Resolution Scheme

The most important step of this simulation is to have a clear and concise collision resolution scheme. This will ensure that the particles land where they are expected. The following collision resolution scheme relies on a 3D ray-traced solution. Since a known velocity vector exists, this vector can be regarded as primary ray from its origin to its final position. As shown in Fig. 2.3, a shadowed region is created by larger particle islands and nucleation sites inside this region are prevented from growing.

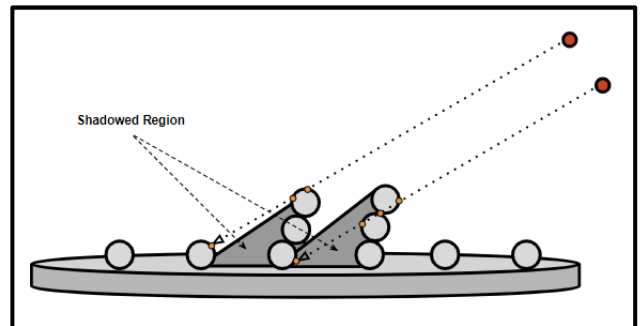


Fig. 2.3: Incoming particles with their cast velocity vectors intersecting with previously deposited particles (in orange)

After the velocity primary ray is cast from its origin source to its destination on the substrate, any intersections with the ray are checked. If an intersection of the ray and a random particle exists, then the final position of the incoming particle is updated. If there are multiple points of intersections, as shown in Fig. 2.3, the point closest to the point of origin is chosen as the final position.

To identify the point of intersection (POI)/collision detection, we took advantage of the fact that particles are represented as spheres. A ray-sphere intersection was used to find that POI. Referring to Fig. 2.4, a ray-sphere intersection is outlined. For a point q_0 , it can be defined as:

$$q_0 = p + t\vec{d} \quad (2)$$

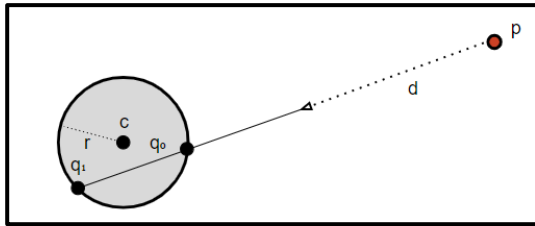


Fig. 2.4: Ray-sphere intersection where d is direction vector

The implicit surface of a sphere is defined as:

$$f(q_0) = (q_0 - c) \cdot (q_0 - c) - r^2 = 0 \quad (3)$$

Using the previous definition of q_0 , the equation for this point on a sphere is as follows:

$$f(p + t\vec{d}) = (p + t\vec{d} - c) \cdot (p + t\vec{d} - c) - r^2 = 0 \quad (4)$$

Simplifying this formula, gives the following result which is of the quadratic form:

$$f(p + t\vec{d}) = (\vec{d} \cdot \vec{d})t^2 + 2\vec{d} \cdot (p - c)t + (p - c) \cdot (p - c) - r^2 = 0 \quad (5)$$

The scalar value, t , can then be found using the quadratic formula where:

$$a = (\vec{d} \cdot \vec{d}), b = 2\vec{d} \cdot (p - c), c = (p - c) \cdot (p - c) - r^2 \quad (6)$$

The smallest value for t is used to find the closest point of intersection. Using (2), this value is then used as a scalar factor to find q_0 , which is the POI of the ray and the sphere. The position of the incoming particle can then be updated to be q_0 . Each incoming particle and its corresponding ray is checked with all previous particles to determine an intersection which creates structures on the substrate.

C. Implementation

To implement this simulation, we wrote our program in Python and utilized the VPython Visual interface. This simulation has a simplified graphical user interface to be able to manipulate the incidence angle, and azimuth rotation angle. We In the near future, we plan to add support for a rotation rate so that continuous structures can be simulated. We simulated ~10,000 particles to form these structures. This number can be dependent on the incidence angle but was kept constant for our purposes. We used 14 monolayers to construct single column growths but for more complex feature growths the number of monolayers can also be modified. Our 3D substrate was of size $1248 \times 1248 \times 48$ pixels. For all the test demonstrations, a standard PC was used to run the simulation.

III. RESULTS AND DISCUSSION

As shown in extensive previous research, the column growth angle (β) and the incidence angle (α) are not the same. This is due to a variety of factors like substrate temperature, pressure, deposition material etc. [2]. Therefore, a comparison between

these two are important in validating the results of the simulation.

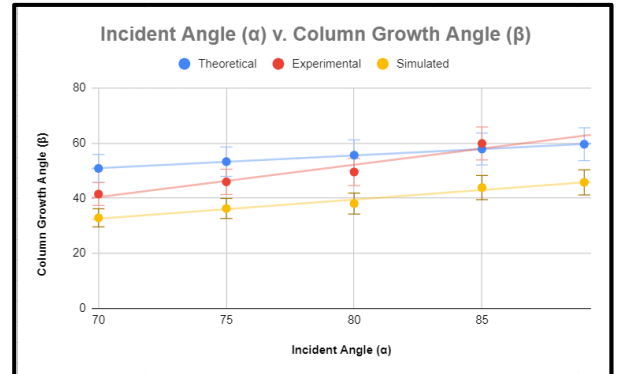


Fig. 3.1: Chart showing different relationship between β and α

Equation (1) was used to find respective theoretical β for each α . In [2], it is also shown that typically $\beta < \alpha$. As shown in Fig. 3.1, the simulated values for β is always less than α . Since our experimental GLAD structures used Germanium as the deposition material, we observed that below 70° , a continuous thin film was formed.

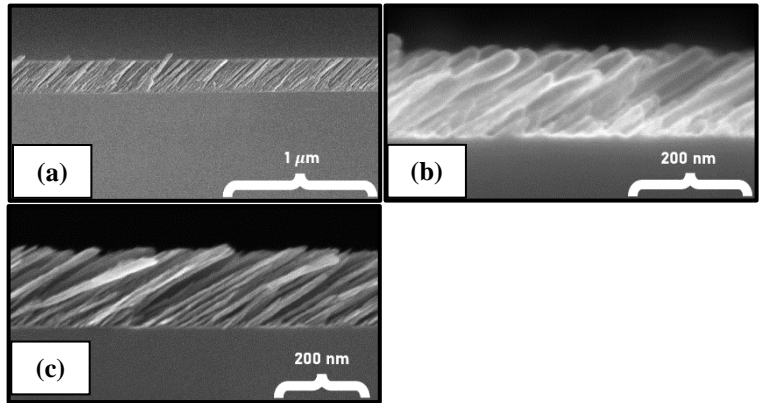


Fig. 3.2: (a) shows column growths at $\alpha = 75^\circ$, (b) shows column growths at $\alpha = 80^\circ$, (c) shows column growths at $\alpha = 85^\circ$

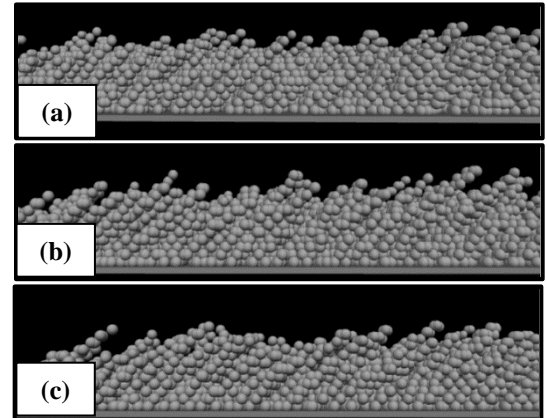


Fig. 3.3: (a) shows simulated column growths at $\alpha = 75^\circ$, (b) shows simulated columns at $\alpha = 80^\circ$, and (c) shows simulated columns at $\alpha = 85^\circ$

As shown in the above figures, a qualitative comparison can be made between the experimental and simulated structures. Doing this, the results are favorable and show that the simulation can be validated for simpler features.

A. Initial Seeding

Up until this point, this paper only mentions the use of natural seeding patterns. Glancing angle deposition also makes the use of initial predetermined seeding patterns. As shown in [4], line seeds, spherical seeds, and column/cube seeds are common pre-seed patterns. Unlike natural seeding, these pre-seeds need to be manually nucleated through processes such as photolithography, focused ion beam, embossing, or other micromachining techniques.

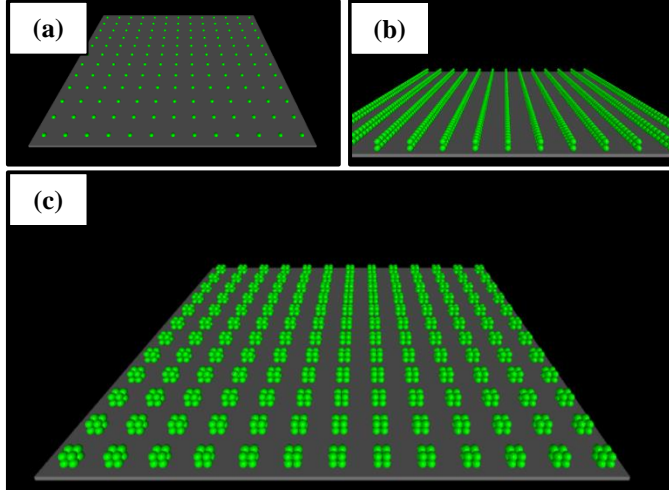


Fig. 3.4: (a) shows simulated spherical seeding pattern, (b) shows simulated line seeding pattern and (c) shows simulated column/cube seeding pattern

Similarly, these results can be compared with our simulated growth results for these initial patterning.

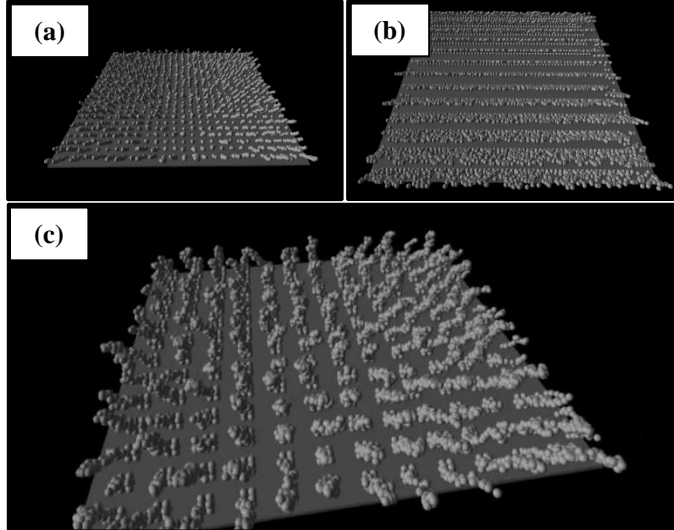


Fig. 3.5: (a) shows simulated spherical seed feature growths, (b) shows simulated line seed feature growths, and (c) shows simulated column/cube seed feature growths

Doing this, seeding patterns can also be simulated for glancing angle deposition. Again, like Fig. 3.2 and Fig. 3.3, a qualitative comparison can be made. The results show very close resemblance to the experimentally produced growths. In our simulations, these patterns were simulated at $\alpha = 80^\circ$. As seen in Fig. 3.5(a) there is a margin of error present between the structures. This is because of the randomness of the points of origin of the incoming vapor particles. The difference between Fig. 3.5(a) and 3.5(c) is that the width of the nanofeatures is much larger for Fig. 3.5(c) than 3.5(a). This is because the seed is much larger, as shown in Fig. 3.4(c). This causes multiple structures to grow on a single seed instead of them growing individually.

Using Fig. 3.1, a quantitative comparison can also be made between the experimental column growths and the incidence angles. Fig. 3.1 shows that our simulation creates a larger difference between the α and β than the experimental values.

Our simulation currently lacks the effect expressed by temperature, chamber pressure, and deposition material. To improve the accuracy of our feature growths we can add additional support for these features. Additionally, a better GUI can be created for enabling an easier use of the different features offered by our simulation. Another important observation is that our features are made up of individual ‘spheres’ representing clusters of atoms. If these spheres are made smaller or are allowed to “fuse” under the right conditions, a very accurate model of the GLAD process can be simulated.

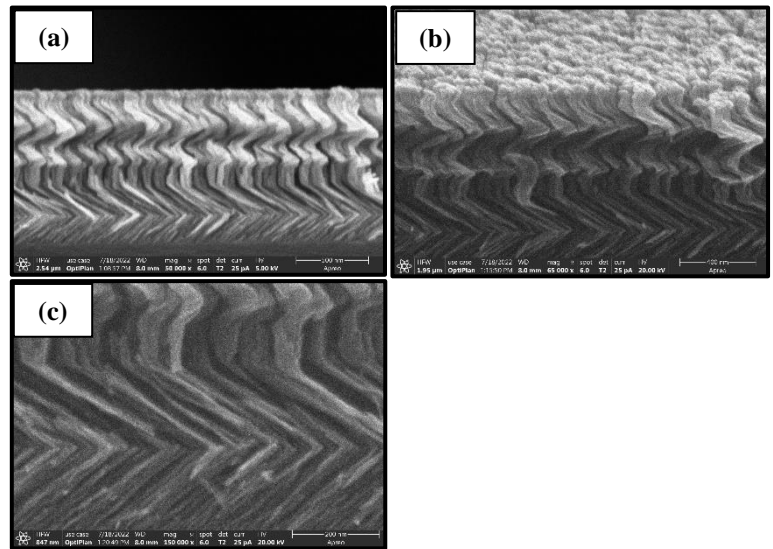


Fig. 3.6: (a) complex structures formed by GLAD – side view, (b) complex structures – tilted view, (c) complex structures – close-up view

B. Complex Structures

We also modelled complex structure growth in our simulation. As expected, the results of these simulations resemble a column on top of a chevron. These structures shown

in Fig. 3.7(a), 3.7(b), 3.7(c) were made using the same parameters as the experimental structures.

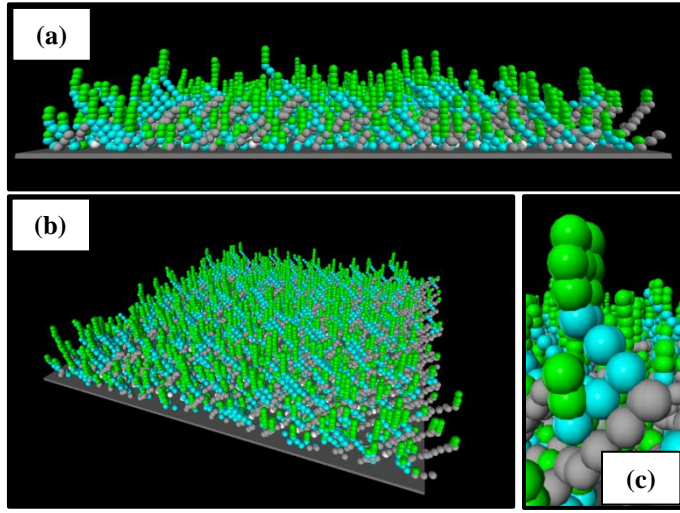


Fig. 3.7: (a) side-view of simulated complex structures, (b) tilted view of simulated complex structures, and (c) individual complex structure

While simulating complex structures, we observed that effects of pre-seeding patterns become insignificant. We hypothesize that this is caused by the treatment of the next columnar structure as landing on a bare substrate.

Another improvement that can be made in simulating complex structures is the addition of a deposition rate. Currently, this rate is constant and only dependent on the incident angle. Adding support for this deposition rate can be used to predict the longevity of experimentally producing these structures.

IV. PROGRAM EFFICIENCY

Our collision resolution algorithm was one of the biggest points of concern in developing this simulation. This algorithm had to be fast enough to be able to simulate a large number of inputs but also accurate enough to be able to resolve collisions for small particles as used here.

Time Complexity	Iterations	Render Time (s)
$O(n^4)$	< 2,500,000,000	38.55
$O(n^3 + n^2)$	< 510,000,000	12.36
$O(n^3 + n)$	< 500,000,000	9.79
$O(sn^3)$	< 100,000,000	3.54

Tab. 1: Shows time complexities, largest number of iterations, and rendering time for each collision resolution algorithm.

As presented in Tab. 1, we tested and presented four different collision resolution algorithms and found that the last one presented was the fastest one. The implementation for each

one was slightly different which explains the differences in the number of iterations even with similar time complexities (TC). The s in each of the algorithms reflect the TCs of the total number of simple features (columns) required to make a complex structure.

V. CONCLUSION

This study demonstrates the use of a Monte-Carlo fashion simulation of glancing angle deposition. We incorporated the VPython package to implement this simulation. We demonstrated the deposition of natural seeds, onto which nanostructures were grown. Our simulation results—growth angle and percent coverage—were demonstrated with respect to inputs such as incidence angle and initial seeding. We further qualitatively compared experimental and simulated results and received favorable results. We also demonstrated the simulation results of complex structures with partially agreeable results.

The simulation results could help predict fabrication results of GLAD for applications in optics, sensing, electronics. We also proposed some new techniques to improve the accuracy of our simulation.

We then demonstrated the characteristics of each of our collision resolution algorithms. We demonstrated the largest iteration count of the collision resolution algorithms which is something that could be taken into consideration when improving the program. Overall, our goal was to develop a 3D-simulation of the GLAD process and we were able to demonstrate it.

ACKNOWLEDGMENTS

This project was supported by the National Science Foundation (NSF) Research Experience for Undergraduates (REU) program at the University of Louisville, Award #ID 1950137; and the KY Multiscale NNCI site, Award #ID 2025075. We would also like to thank the MNTC for their support in fabrication.

REFERENCES

- [1] B. Dick, M. J. Brett, T. J. Smy, M. R. Freeman, M. Malac, and R. F. Egerton, “Periodic magnetic microstructures by glancing angle deposition,” *Journal of Vacuum Science & Technology A: Vacuum, Surfaces, and Films*, vol. 18, no. 4, pp. 1838–1844, Jul. 2000, doi: [10.1116/1.582481](https://doi.org/10.1116/1.582481).
- [2] M. Taschuk, M. Hawkeye, M. Brett, *Handbook of Deposition Technologies for Films and Coatings*, William Andrew Publishing, 2010. p. 625.
- [3] B. C. Hubart, X. Liu, and J. G. Amar, “Large-scale molecular dynamics simulations of glancing angle deposition,” *Journal of Applied Physics*, vol. 114, no. 8, p. 083517, Aug. 2013, doi: [10.1063/1.4819446](https://doi.org/10.1063/1.4819446).
- [4] C. Qu, B. Alphenaar, S. McNamara, and K. Walsh, “Design of line seeds for glancing angle deposition,” *Journal of Vacuum Science & Technology A*, vol. 39, no. 4, p. 043404, Jul. 2021, doi: [10.1116/6.0000998](https://doi.org/10.1116/6.0000998).